AN EFFICIENT CONTROL FOR A STANDALONE PHOTOVOLTAIC WATER PUMPING SYSTEM BASED ON A SEPARATELY EXCITED DC MOTOR DRIVE

Samir Zoughab[1]* – Nouri Belhaouchet[1] – Samir Sayah[2]

[1]LAS Laboratory, Department of Electrical Engineering, Faculty of Technology, Setif 1 University-Ferhat Abbas, Campus EL Maabouda, 19000 Setif, Algeria
[2]QUERE Laboratory, Department of Electrical Engineering, Faculty of Technology, Setif 1 University-Ferhat Abbas, Campus EL Maabouda, 19000 Setif, Algeria

ARTICLE INFO	Abstract:
	This paper deals with a simple and efficient control for a standalone photovoltaic (PV) water pumping system based on a separately excited DC motor drive. The structure of this system uses two power converters coupled by a DC-bus capacitor. The first is a DC-DC boost converter used to extract the available maximum power of the PV array by using a perturb-and-observe maximum power point tracking (P&O MPPT) technique. The second is a DC-DC buck converter used as an interface to supply the armature circuit of the DC motor with a variable voltage according to the produced PV power. In order to ensure a constant magnetic flux, the field circuit of the DC motor is connected to the DC-bus capacitor and the DC-bus voltage is regulated at a desired level. The main advantage of this structure is that the features of an expensive permanent magnet DC motor can be achieved by using a low cost separately excited DC motor. The usefulness of this system is verified by a digital simulation using Matlab/Simulink and experimentally confirmed by a real-time implementation based on dSPACE 1104 system card. The illustrated results show a good agreement between simulations and experiments for various operating conditions.

1 Introduction

In recent years, the excessive use of non-renewable energy resources for electricity generation leads to serious environmental problems in the world. These problems inevitably rise increasingly especially with the increasing of the economic growth. Therefore, in order to reduce these environmental impacts, significant amounts of efforts are being taken by the most country of the world to the development of renewable energies. Among several renewable energy sources currently used, the solar photovoltaic (PV) energy is becoming an alternative source to the non-renewable energy sources. It has an inexhaustible nature and an abundant availability and represents a strategic solution for overall social development [1]. It is well known that the output voltage and current of a solar PV array are non-linearly related, this induces a non-linear Power-Voltage characteristic which has only one peak called maximum power point (MPP). This MPP depends on different factors such as solar irradiance and temperature. Therefore, the direct coupling without power conditioning leads to a poor efficiency. To extract the MPP at any atmospheric condition, it is necessary to make the power conditioning by using an intermediate power conditioning unit equipped with a maximum power point tracking (MPPT) technique [2]-[4]. The PV systems are typically operated as standalone (off-grid) [5]-[15], hybrid [16], [17] and grid-connected systems (on-grid) [1], [18]-[20]. The

---

* Corresponding author
E-mail address:samir.zoughab@univ-setif.dz

standalone PV systems are widely used in remote regions, where these installations are independent of the local grid; they are used to meet small essential electric power requirements. The standalone PV systems can use storage systems like batteries to store the produced energy during daytime and provide it to electrical loads during nighttime or cloudy days (to ensure a continuous power supply to the loads), or simply use the produced energy only during the daytime without electrical energy storage.

The PV water pumping is one of most applications of the standalone PV systems. It's important for domestic use and irrigation purpose. Different types of motors are used in PV water pumping systems to drive the pump [8]-[15]. Among these motors, permanent magnet DC motor, despite being expensive, is the most popular choice for PV water pumping systems [8], [13]. In this work, a standalone PV water pumping system is investigated. This system uses a separately excited DC motor to drive a centrifugal pump. The main contribution of this research work is the development of a simple conversion structure for a good adaptation of this drive to the PV array. The structure of this system uses two power converters linked by a DC-bus capacitor to which the field circuit of this motor is connected. The first is a DC-DC boost converter, used as an intermediate power-conditioning unit to extract the maximum power of the PV array by using a perturb-and-observe maximum power point tracking (P&O MPPT) technique. The P&O algorithm is largely employed for its simplicity of implementation, the acceptable response time, its lower cost and it is suitable for the PV applications. Other researchers have developed many MPPT methods based on different ideas [2], [3], [14], [15]. Example [15] uses a variable step size P&O-based CMPPT technique which can reduce the steady-state PV power fluctuation and accelerate the tracking operation under sudden irradiance change, but it is more complex than P&O-based MPPT method.

The second is a DC-DC buck converter used to supply the armature circuit. The DC-bus voltage is regulated at a required level to ensure a constant magnetic flux. With this structure, the separately excited DC motor has a main advantage of being easily controlled; the flux and torque are naturally decoupled and are independently controlled. The field circuit consumes a constant current while the armature current varies according to the load and the PV power which depends on the atmospheric conditions. Therefore, the characteristics of an expensive permanent magnet DC motor can be achieved by using a low-cost separately excited DC motor. Globally, low-cost and simplicity are the advantages of this drive. The usefulness of this application is verified by a digital simulation under the Matlab/Simulink environment and validated in real-time via a test bench prototype based on a dSPACE 1104 board. The remainder of this paper is organized as follows. Section 2 introduces the configuration of the PV water pumping system. Section 3 presents the mathematical model of PV module and motor-pump group. The design of the PV array, the DC-DC boost converter and the centrifugal pump is given in section 4. The control strategy of the PV water pumping system is described in section 5. The simulation and the experimental validation of the PV water pumping system are given in section 6. The last section presents some conclusions.

2   PV water pumping system

The PV water pumping system shown in Figure 1 contains two power converters. The first is a DC-DC boost converter connected to the PV array; employed as an intermediate power-conditioning unit, while the second is a DC-DC buck converter allows to supply the armature circuit with a variable voltage. The two converters are coupled via a DC-bus capacitor. The field circuit of the DC motor is connected to the DC-bus capacitor. A rheostat is added in series with the field circuit to adjust the field current at its rated value.

3   Modeling of PV module and motor-pump group

3.1 PV module modeling

The equivalent circuit of a PV cell is shown in Figure 2. The current-voltage characteristic of a PV cell is given by [21]-[23]:

$$I = I_{ph} - I_0 \left[\exp\left(\frac{q\left(V + R_s I\right)}{A K_B T} \right) - 1 \right] - \frac{V + R_s I}{R_{sh}} \tag{1}$$

Where I_{ph} is the photo-current, I_0 is the reverse saturation current, q is the electron charge, A is the ideality factor of the diode, K_B is the Boltzmann's constant, T is the PV cell temperature, R_s is the series resistance and R_{sh} is the shunt resistance.
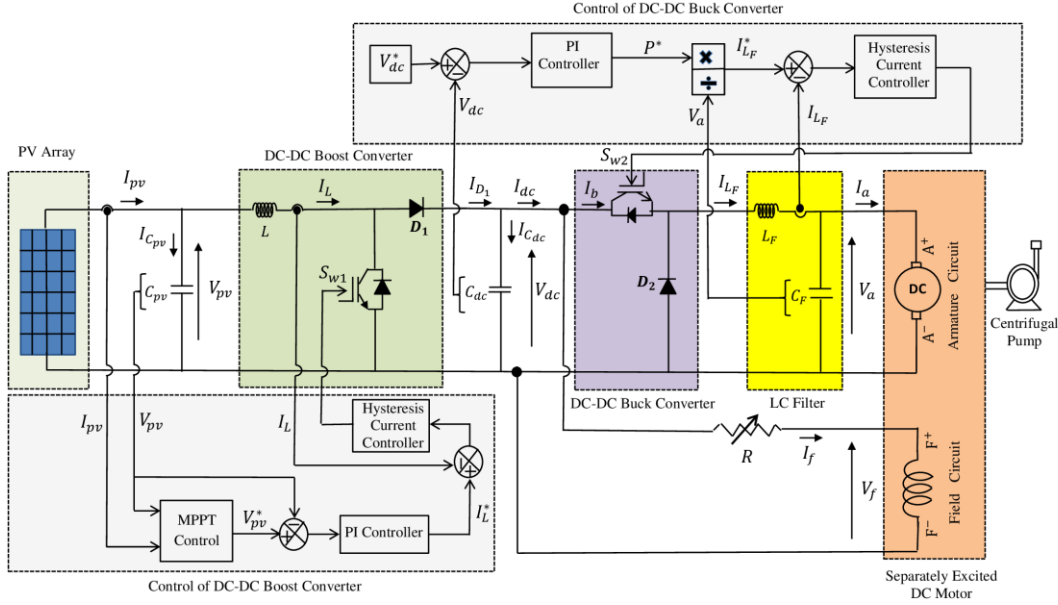

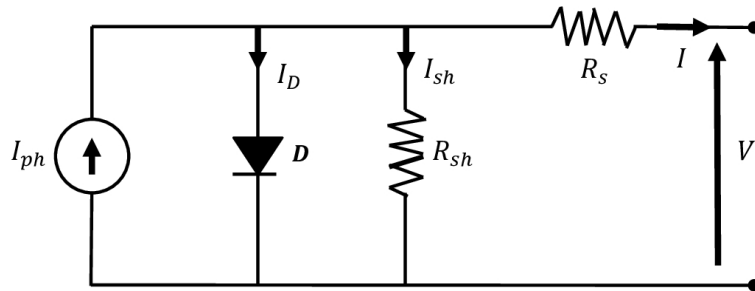Figure 1. PV water pumping system structure.

Figure 2. Equivalent circuit of a PV cell.

The photo-current is expressed as follows:

$$I_{ph} = \frac{E}{E_r}\left(I_{scr} + \alpha_I\left(T - T_r\right)\right) \tag{2}$$

Where E is the solar irradiance, E_r and T_r are respectively the solar irradiance and the cell temperature at standard test conditions STC (E_r = 1000 W/m² and T_r = 25°C), I_{scr} is the short-circuit current of the PV cell at STC, α_I is the short-circuit current temperature coefficient.
The reverse saturation current of the diode is expressed as:

$$I_0 = I_{0r}\left[\frac{T}{T_r}\right]^3 \exp\left[\frac{qE_g}{AK_B}\left(\frac{1}{T_r} - \frac{1}{T}\right)\right] \tag{3}$$

Where E_g is the energy band gap, I_{0r} is the reverse saturation current of the diode at STC given by:

$$I_{0r} = \frac{I_{scr}}{\exp\left(\dfrac{qV_{ocr}}{AK_BT_r}\right) - 1} \tag{4}$$

Where V_{ocr} is the open circuit voltage of PV cell at STC.

The PV module is generally constructed by connecting N_s series cells and N_p parallel cells. So, the output voltage and the output current of a PV module can be expressed by:

$$\begin{cases} V_{mpv} = N_s V \\ I_{mpv} = N_p I \end{cases} \tag{5}$$

Where V_{mpv} and I_{mpv} are respectively the voltage and current generated by the PV module.

The output current of a PV module can be given by:

$$I_{mpv} = N_p I_{ph} - N_p I_o \left[\exp\left(\frac{q\left(V_{mpv} + \dfrac{N_s}{N_p}R_s I_{mpv}\right)}{N_s A K_B T}\right) - 1\right] - \frac{V_{mpv} + \dfrac{N_s}{N_p}R_s I_{mpv}}{\dfrac{N_s}{N_p}R_{sh}} \tag{6}$$

3.2 Motor-pump group modeling

The separately excited DC motor model can be given by:

$$\begin{cases} V_f = R_f I_f + L_f \dfrac{dI_f}{dt} \\[2mm] V_a = R_a I_a + L_a \dfrac{dI_a}{dt} + E \\[2mm] E = k_e \Omega = L_{af} I_f \Omega \\[2mm] T_e = k_t I_a = L_{af} I_f I_a \\[2mm] J \dfrac{d\Omega}{dt} = T_e - f\Omega - T_L \end{cases} \tag{7}$$

Where V_f and I_f are respectively the voltage and the current of the field circuit, V_a and I_a are respectively the voltage and the current of the armature circuit, R_f and R_a are respectively the field resistance and armature resistance, L_f and L_a are respectively the field inductance and armature inductance, L_{af} is the field-armature mutual inductance, Ω is the motor speed, E is the back-emf, T_e is the electromagnetic torque, T_L is the load torque, k_e is the coefficient of back-emf, k_t is the coefficient of electromagnetic torque, J is the inertia and f is the friction coefficient.

According to the available PV power, the centrifugal pump runs at various speeds. The power-speed characteristic of the centrifugal pump can be given by [12]:

$$P_{out} = k_p \Omega^3 \tag{8}$$

Where k_p is the proportionality constant.

4   System design

The PV array should be chosen to deliver a maximum power at STC more than the rated power of the separately excited DC motor which drives the centrifugal pump. The excess of this PV power can compensate the losses of the used converters and the DC motor. The DC-DC boost converter is controlled by a closed loop control such that it forces the PV array to operate at its MPP and also it generates a fixed output DC voltage. The latter, from its input voltage imposed by the PV array $V_{pv} = V_{pv_{mpp}}$, it must deliver an output voltage (the DC-bus voltage) V_{dc} a little bit taller than the rated voltage of the armature circuit of the DC motor. This offers a minimal value of the duty cycle, which meets these requirements, expressed as [5]:

$$d = \frac{V_{dc} - V_{pv_{mpp}}}{V_{dc}} \qquad (9)$$

Where: $V_{pv_{mpp}}$ is the output voltage of the PV array at MPP.
The inductance and the capacitance can be estimated by:

$$L = \frac{V_{pv} d}{\Delta I_L f_s} \qquad (10)$$

$$C_{dc} = \frac{I_{dc} d}{\Delta V_{dc} f_s} \qquad (11)$$

Where f_s is the switching frequency, ΔI_L is the ripple of the inductor current, ΔV_{dc} is the ripple of the capacitor voltage.
The centrifugal pump can be designed from DC motor rating as [12]:

$$k_p = \frac{P_{outn}}{\Omega_n^3} \qquad (12)$$

Where p_{outn} and Ω_n are respectively the rated output power and the rated speed of motor.

5   Control strategy

5.1   DC-DC boost converter control

As shown in Figure 1, the control system of this stage contains two control loops (outer and inner). The outer loop uses a proportional-integral (PI) controller to regulate the voltage V_{pv} at its reference value V_{pv}^* and provide the reference inductor current I_L^* [24]. The reference value V_{pv}^* is generated continuously by using an MPPT technique based on P&O algorithm represented by its flowchart shown in Figure 3 [2].
From Figure 1, the capacitor current $I_{C_{pv}}$ is given by [24]:

$$I_{C_{pv}} = I_{pv} - I_L = C_{pv} \frac{dV_{pv}}{dt} \qquad (13)$$

By neglecting I_{pv} (considered as disturbance) and utilizing the Laplace transform, (13) becomes:

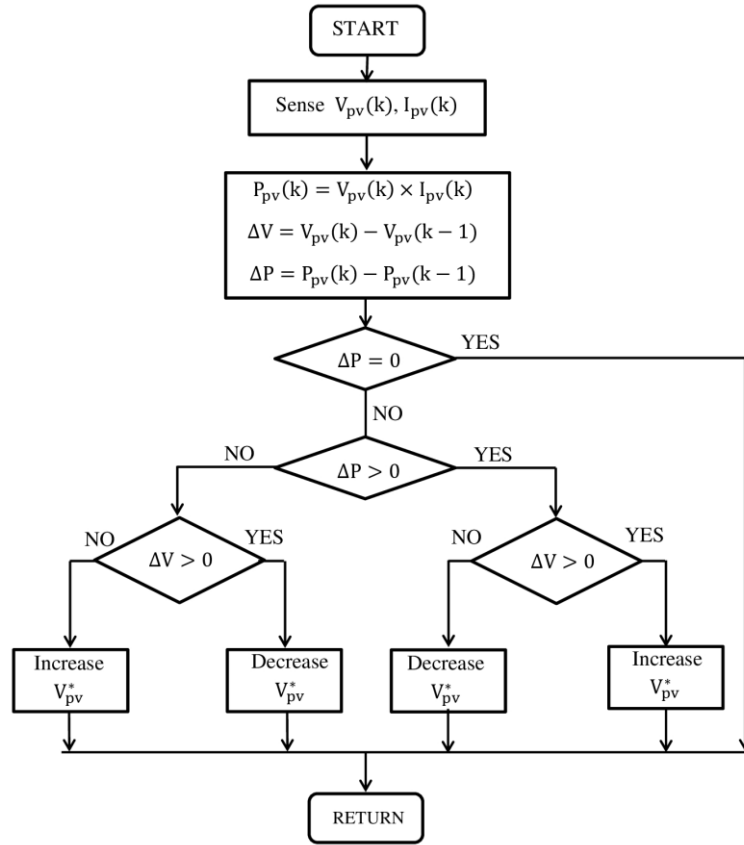$$I_{C_{pv}}(s) = -I_L(s) = C_{pv} s V_{pv}(s) \qquad (14)$$

Figure 3. Flowchart of P&O MPPT algorithm.

For a faster current loop, it can be considered that $I_L = I_L^*$, so the closed-loop control of the voltage V_{pv} can be presented as in Figure 4.
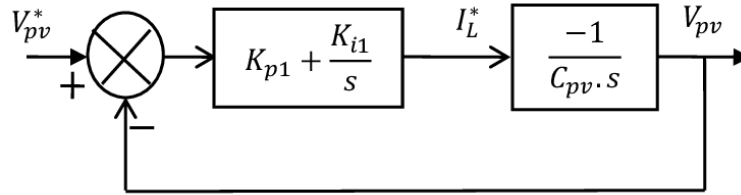

Figure 4. Closed-loop control of the PV array output voltage.

The closed-loop transfer function $G_1(s)$ of the system shown in Figure 4 is given by:

$$G_1(s) = \frac{s\,K_{P1} + K_{i1}}{-s^2 C_{pv} + s\,K_{p1} + K_{i1}} \tag{15}$$

Writing $G_1(s)$ in its standard form, the gains of PI controller can be calculated as:

$$\begin{cases} K_{p1} = -2\xi C_{pv}\omega_n \\ K_{i1} = -C_{pv}\omega_n^2 \end{cases} \tag{16}$$

Where ξ, ω_n are respectively the damping ratio and natural angular frequency.

For the inner loop, a hysteresis current controller (HCC) is used. The HCC will force the inductor current I_L to track the reference current I_L^*. This controller is characterized by simplicity, rapidity and high robustness.

5.2 Separately excited DC motor control

In this system, a centrifugal pump is driven by a separately excited DC motor. The power of the DC motor has a direct relationship with its speed. Therefore, the PV power and the speed of the DC motor are both affected by variations of atmospheric conditions. As shown in Figure 1, the field circuit of the DC motor is connected to the DC-bus capacitor and the armature circuit is supplied by a DC-DC buck converter. The control circuit uses a PI controller which ensures the regulation of the DC-bus voltage and an HCC which forces the inductor current I_{L_F} to track the reference current $I_{L_F}^*$. This control regulates the magnetic flux at its rated value and activates the DC-DC buck converter which continuously adjusts the armature voltage. The PI controller minimizes the error between the DC-bus voltage V_{dc} and the reference voltage V_{dc}^* and generates the reference power P^* to be transferred to the armature circuit.

From Figure 1, by neglecting the current of the field circuit I_f, the DC-DC buck converter input current is given by:

$$I_b = I_{dc} = I_{D_1} - I_{C_{dc}} \tag{17}$$

By neglecting the disturbance term I_{D_1}. In Laplace transform form, (17) becomes:

$$I_b(s) = -I_{C_{dc}}(s) = C_{dc}\, s\, V_{dc}(s) \tag{18}$$

The relationship between the DC-bus voltage and the generated reference power can be expressed as:

$$P^* = -V_{dc}^*\, C_{dc}\, s\, V_{dc} \tag{19}$$

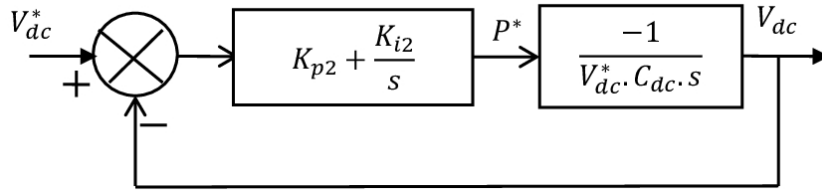The closed-loop control of the DC-bus voltage is shown in Figure 5.

Figure 5. Closed-loop control of the DC-bus voltage.

The closed-loop transfer function $G_2(s)$ of the system presented in Figure 5 is given by:

$$G_2(s) = \frac{s\, K_{p2} + K_{i2}}{-s^2 C_{dc} V_{dc}^* + s\, K_{p2} + K_{i2}} \tag{20}$$

Writing $G_2(s)$ in its standard form, the gains of the PI controller can be defined as:

$$\begin{cases} K_{p2} = -2\,\xi\, C_{dc} V_{dc}^* \omega_n \\ K_{i2} = -C_{dc} V_{dc}^* \omega_n^2 \end{cases} \tag{21}$$

Where ξ, ω_n are the damping ratio and natural angular frequency respectively.

The reference current $I_{L_F}^*$ can be obtained by:

$$I_{L_F}^* = \frac{P^*}{V_a}$$
(22)

The current I_{L_F} which has the same average value of the armature current is forced to track its reference $I_{L_F}^*$ by an HCC.

6   Simulation and experimental validation

6.1 Parameters of PV water pumping system

The employed PV array is composed of two identical PV modules connected in series. Each PV module has the specifications presented in table 1.

Table 1. Specifications of the PV module at STC.

Description	Value
Maximum power point	85 W
Open circuit voltage	22.2 V
Short circuit current	5.15 A
Voltage at maximum power point	17.8 V
Current at maximum power point	4.8 A

The Current-Voltage and Power-Voltage curves obtained by simulation of the used PV array at STC (solar irradiance 1000 W/m^2 and cell temperature 25 °C) are shown in Figure 6.
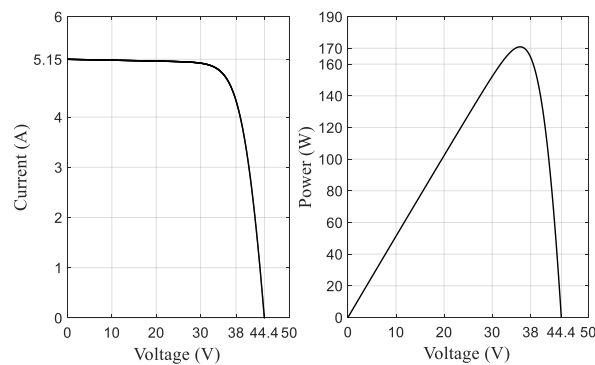

Figure 6. Characteristics of the PV array at STC.

The specifications of the separately excited DC motor are presented in table 2.

Table 2. Separately excited DC motor ratings.

Description	Value
Rated power	100 W
Rated speed	2000 rpm
Rated armature voltage	220 V
Rated armature current	0.63 A
Rated voltage of field-circuit	220 V
Rated current of field-circuit	0.08 A

The power circuit parameters are shown in table 3.

Table 3. Power circuit parameters.

Parameters	Description	Value
V_{dc}	DC-bus voltage	240 V
R	Rheostat	250 Ohms
C_{pv}	Output PV array capacitor	200 µF
C_{dc}	DC-bus capacitor	1100 µF
L	Inductor of boost converter	10 mH
L_F, C_F	Output LC Filter	200 mH, 1100 µF

The proportionality constant of the centrifugal pump is calculated as:

$$k_p = \frac{P_{outn}}{\Omega_n^3} = \frac{100}{\left(\dfrac{2000 \times \pi}{30}\right)^3} = 1,088 \times 10^{-5} \, W/(rd/s)^3$$

6.2 Laboratory experimental test bench

The experimental test bench developed in the laboratory is shown in Figure 7. The separately excited DC motor which drives the centrifugal pump is fed by a PV array. The PV array comprises two identical PV modules connected in series. The conversion structure uses two power converters (DC-DC boost converter and DC-DC buck converter) based on IGBT modules. The two converters are linked via a DC-bus capacitor to which the field circuit of the DC motor is connected. The rheostat added in series with the field circuit permits to set the voltage of this circuit at its rated value 220 V. The program of the control system is digitally implemented in real-time by using a dSPACE1104 system card with a sampling time of 60 µs. The control system necessities three voltage sensors (to detect the output voltage of the PV array, the armature voltage and the DC-bus voltage), and three Hall Effect current sensors (to detect the PV output current, the inductor current of the DC-DC boost converter and the filter inductor current on the output of DC-DC buck converter). Other modules are integrated to ensure the insulation of the control signals.

6.3 Simulation and experimental results

The performances of the PV water pumping system are examined by several simulation and experimental tests. The simulation tests are performed by taking into consideration the same conditions of the experimental tests realized at real atmospheric conditions.

6.3.1 Starting performances

This test is realized to show the starting performances of the PV water pumping system. The PV array operates under the atmospheric conditions (900 W/m²; 70 °C). The electrical quantities (voltage, current, power) of the PV array and the motor speed are shown in Figure 8 (simulation results (Figure 8-a) and the experimental results (Figure 8-b)). These results show that after a short transient of 2 s, the MPPT technique ensures the operating with a maximum power of 123 W and the DC motor drives the centrifugal pump with a speed of 1570 rpm. The starting of the separately excited DC motor makes a delay of 1 s. This delay is due to the DC-bus voltage which initially has a very weak value (37 V), where the magnetic flux is very weak, this leads to a very low starting torque.

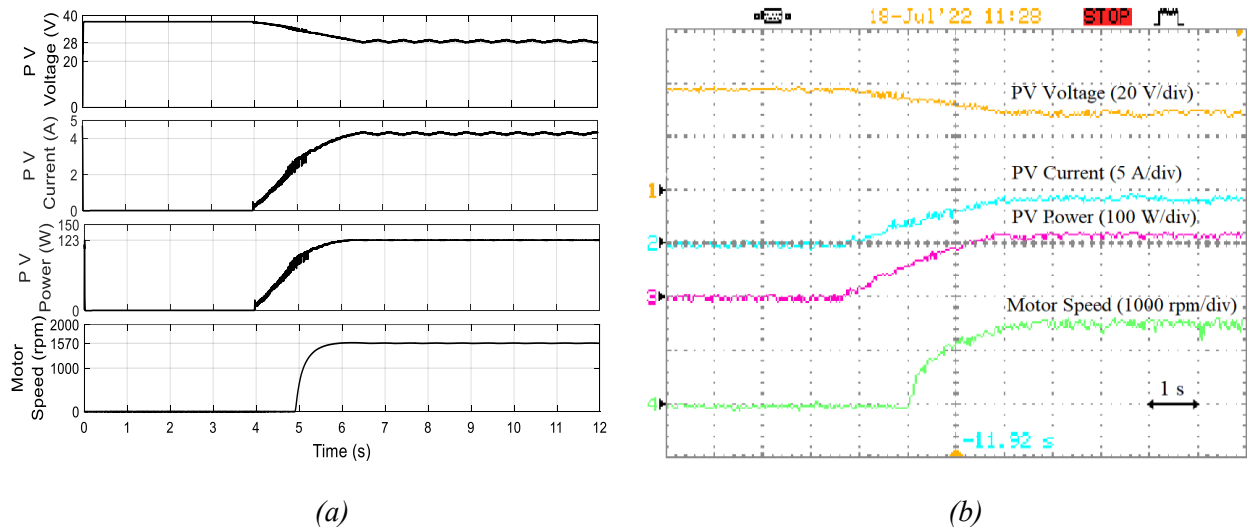*Figure 7. Experimental test bench based on dSPACE 1104.*

(a)   *(b)*

Figure 8. Performances of the PV water pumping system at starting: (a) Simulation results, (b) Experimental results.

6.3.2   Steady-state performances

The goal of this test is to show the performances of the PV water pumping system in steady-state. The system operates with atmospheric conditions (780 W/m²; 70 °C). Figure 9 shows the waveforms of the DC-bus voltage, the armature voltage, the generated PV power and the motor speed. From these results, it is well observed that the PV array generates a power of 105 W. The DC-bus voltage is well regulated around the imposed value 240 V; this offers a constant magnetic flux. The DC-DC buck converter adjusts the armature voltage to 160 V and the DC motor drives the centrifugal pump with a speed of 1500 rpm.
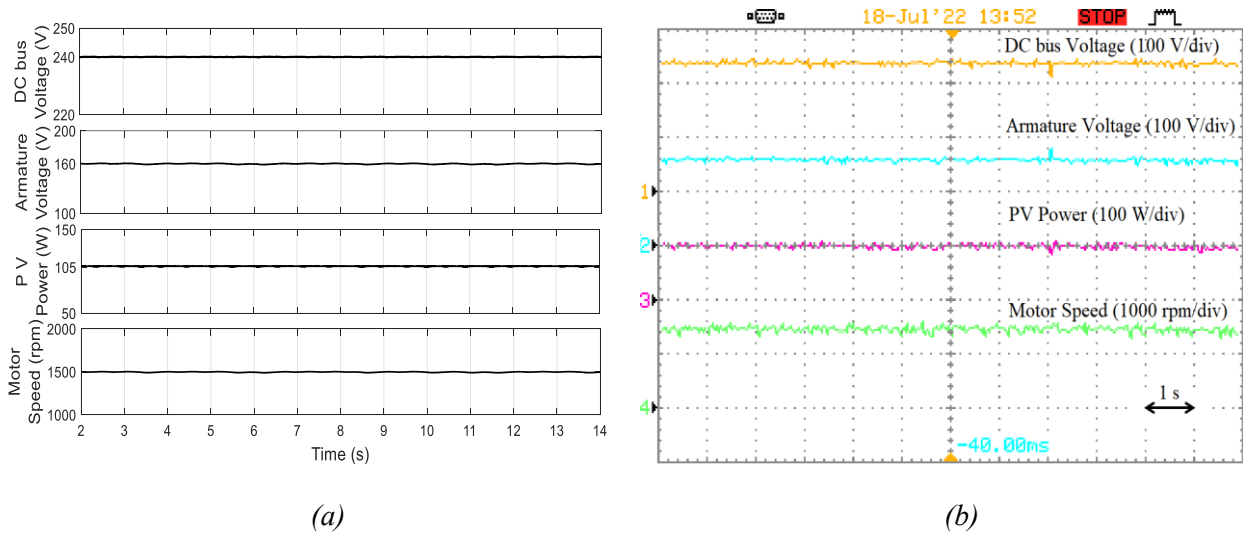
(a)   *(b)*

Figure 9. Performances in steady-state of the PV water pumping system: (a) Simulation results; (b) Experimental results.

6.3.3   Performances of the PV water pumping system for disconnection and reconnection of the PV array

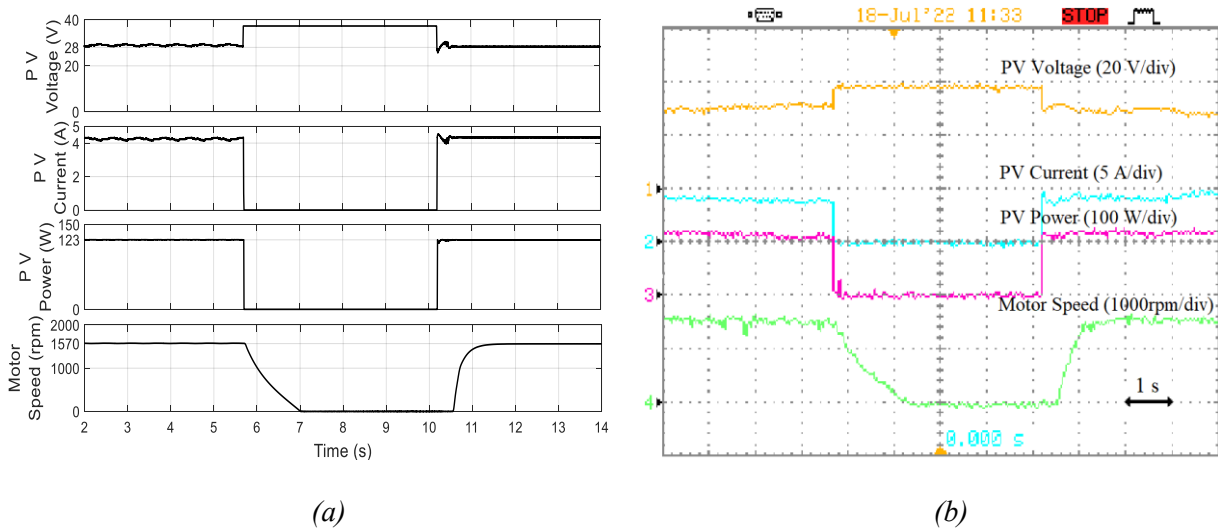*(a)*   *(b)*

Figure 10. System response during disconnection and reconnection of the PV array: (a) Simulation results, (b) Experimental results.

The aim of this test is to illustrate the system response for a disconnection and then a reconnection of the PV array. The system operates with atmospheric conditions (900 W/m²; 70°C). Figure 10 shows the waveforms of the PV voltage, the PV current, the generated PV power and the motor speed. From these results, it is clearly observed that the PV array generates a power of 123 W to the DC motor which drives the centrifugal pump at 1570 rpm. At the time of the disconnection, the generated PV power directly decreases to zero, the PV voltage increases and then stabilities at the open circuit voltage value. After 1.2 s the DC motor is stopped. At the time of the reconnection, the MPPT control rapidly recuperates its functioning and tracks the available maximum power (123 W), the DC motor restarts and drives the centrifugal pump at 1570 rpm.

6.3.4   Performances of the PV water pumping system for connection and disconnection of a resistive load in parallel with the PV array

The purpose of this test is to study a behavior like to a fast variation in solar irradiance. In this case, the PV array operates under (800 W/m²; 70 °C), then after a while a resistive load of 20 Ω which consumes 40 W is connected in parallel with the PV array and then disconnected. The waveforms of the PV voltage, the

PV current, the produced PV power and the motor speed are shown in Figure 11. From these results, it can be seen that the MPPT technique has a very good dynamic response facing these sudden variations. At times of connection and disconnection of the resistive load, the output PV voltage is practically not affected, while sudden decrease and increase in the output PV current are presented. Before the connection of the resistive load, the PV array provides to the DC motor a power of 109 W and the centrifugal pump is driven at 1515 rpm. After the addition of this resistive load, the produced PV power becomes 70 W and the DC motor drives the centrifugal pump at 1220 rpm.
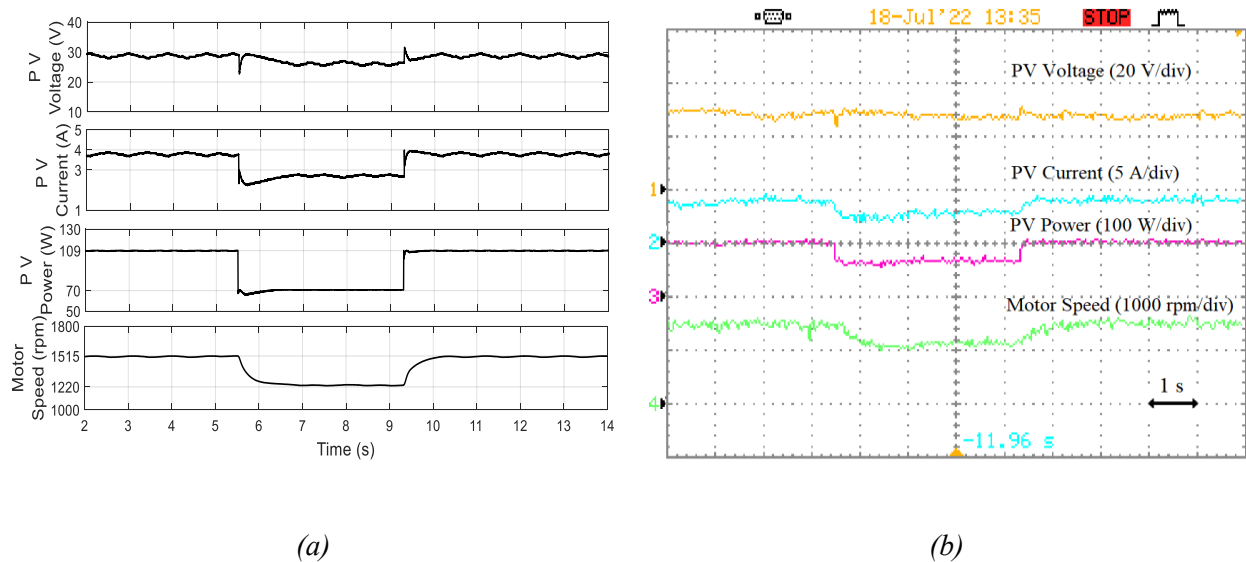

(a) *(b)*

Figure 11. System response for connection and disconnection of a resistive load in parallel with the PV array: (a) Simulation results, (b) Experimental results.

7   Conclusion

This paper has described a high-performance standalone PV water pumping system based on a separately excited DC motor drive. The conversion structure ensures the extraction of the available PV array maximum power and the transmission of the produced PV power to the DC motor. It contains two DC-DC converters associated with a DC-bus capacitor to which the field circuit of the DC motor is connected. The first is a DC-DC boost converter dotted with P&O MPPT technique and the second is a DC-DC buck converter used to supply the armature circuit with a variable voltage. The DC-bus voltage is regulated at a desired level to ensure a constant magnetic flux. The usefulness of the PV water pumping system was verified by a digital simulation and experimentally confirmed by a real-time implementation using dSPACE1104 system card. A good agreement was observed between the experimental results and the simulation results. The obtained results have demonstrated that the used system is characterized by good performances for steady-state and transient responses.

References

[1]   A. Kharrazi, V. Sreeram, and Y. Mishra, "Assessment techniques of the impact of grid-tied rooftop photovoltaic generation on the power quality of low voltage distribution network-A review," *Renew. Sustain. Energy Rev*., vol. 120, pp. 109643, 2020, doi: 10.1016/j.rser.2019.109643.

[2]   A. K Podder, N. K Roy, and H.R Pota,"MPPT methods for solar PV systems: a critical review based on tracking nature," *IET Renew. Power Gener*., vol. 13, no. 10, pp. 1615-1632, 2019, doi: 10.1049/iet-rpg.2018.5946.

[3]   M. Mao, L. Cui, Q. Zhang, K. Guo, L. Zhou, and H. Huang, "Classification and summarization of solar photovoltaic MPPT techniques: A review based on traditional and intelligent control strategies,"*Energy Rep*., vol. 6, pp. 1312-1327, 2020, doi: 10.1016/j.egyr.2020.05.013.

[4]   V. R Vakacharla, K. Gnana, P. Xuewei, B. L. Narasimaharaju, M. Bhukya, A. Banerjee, R. Sharma,

and A. K. Rathore, "State-of-the-art power electronics systems for solar-to-grid integration,"*Sol. Energy*., vol. 210, pp. 128-148, 2020, doi: 10.1016/j.solener.2020.06.105.

[5]   M. Dubey, S. K. Sharma, and R. Saxena, "Cascaded boost buck converter for solar power driven stand-alone PMSM drive,"*Renew. Energy Focus*., vol. 35, pp. 32-40, 2020, doi: 10.1016/j.ref.2020.07.001.

[6]   J. Meyer, and S. von Solms, "Design Considerations for Reducing Battery Storage in Off-Grid, Stand-Alone, Photovoltaic-Powered Cold Storage in Rural Applications," *Energies*,vol. 15, no. 9, pp. 3468, 2022, doi: 10.3390/en15093468.

[7]   E. Guerrero-Ramirez, A. Martinez-Barbosa, M. A. Contreras-Ordaz, G. Guerrero-Ramirez, E. Guzman-Ramirez, L. J. Barahona-Avalos, andM. Adam-Medina, "DC motor drive powered by solar photovoltaic energy: An FPGA-based active disturbance rejection control approach,"*Energies*, vol. 15, no. 18, pp. 6595, 2022, doi: 10.3390/en15186595.

[8]   A. Tariq, and M. J. Asghar, "Matching of a separately excited dc motor to a photovoltaic panel using an analog maximum power point tracker,"*In 2006 IEEE Int. Conf. Ind. Technol*., pp. 1020-1025,2006, doi: 10.1109/ICIT.2006.372281.

[9]   M. M. Ahmed, W. S. Hassanien, and M. A. Enany, "Modeling and evaluation of SC MPPT controllers for PVWPS based on DC motor,"*Energy Rep.*, vol. 7, pp. 6044-6053, 2021, doi: 10.1016/j.egyr.2021.09.055.

[10] I. Saady, M. Karim, B. Bossoufi, N. El Ouanjli, S. Motahhir, and B. Majout, "Optimization and control of photovoltaic water pumping system using kalman filter based MPPT and multilevel inverter fed DTC-IM,"*Results Eng.*, vol. 17, pp. 100829, 2023, doi: 10.1016/j.rineng.2022.100829.

[11] G. H. K. Varma, V. R. Barry, and R. K Jain, "A total-cross-tied-based dynamic photovoltaic array reconfiguration for water pumping system,"*IEEE Access*, vol. 10, pp. 4832-4843, 2022, doi: 10.1109/ACCESS.2022.3141421.

[12] S. Murshid, and B. Singh, "Single stage autonomous solar water pumping system using PMSM drive,"*IEEE Trans. Ind. Appl*., vol. 56, no. 4, pp. 3985-3994, 2020, doi: 10.1109/TIA.2020.2988429.

[13] V. C. Sontake, V. R. Kalamkar, "Solar photovoltaic water pumping system-A comprehensive review,"*Renew. Sustain. Energy Rev*., vol. 59, pp. 1038-1067, 2016, doi: 10.1016/j.rser.2016.01.021.

[14] A. Narendra, N. V. Naik, A. K. Panda, and N. Tiwary, "A comprehensive review of PV driven electrical motors,"*Sol. Energy*, vol. 195, pp. 278-303, 2020, doi: 10.1016/j.solener.2019.09.078.

[15] B. Talbi, F. Krim, T. Rekioua, S. Mekhilef, A. Laib, and A. Belaout "A high-performance control scheme for photovoltaic pumping system under sudden irradiance and load changes,"*Sol. Energy*, vol. 159, pp. 353-368, 2018, doi: 10.1016/j.solener.2017.11.009.

[16] W. Obaid, A. K. Hamid, and C. Ghenai, "Hybrid water pumping system design: A case study in Dubai, United Arab Emirates," *Case Stud. Therm. Eng*., vol. 26, pp. 101121, 2021, doi: 10.1016/j.csite.2021.101121.

[17] G. Zhang, W. Hu, D. Cao, W. Liu, R. Huang, Q. Huang, Z. Chen, and F. Blaabjerg, "Data-driven optimal energy management for a wind-solar-diesel-battery-reverse osmosis hybrid energy system using a deep reinforcement learning approach,"*Energy Convers. Manag*., vol. 227, pp. 113608, 2021, doi: 10.1016/j.enconman.2020.113608.

[18] R. Panigrahi, S. K. Mishra, S. C. Srivastava, A. K. Srivastava, and N. N. Schulz, N, N, "Grid integration of small-scale photovoltaic systems in secondary distribution network—A review,"*IEEE Trans. Ind. Appl*., vol. 56, no. 3, pp. 3178-3195, 2020, doi: 10.1109/TIA.2020.2979789.

[19] S. Mishra, D. Pullaguram, S. A. Buragappu, and D. Ramasubramanian, "Single-phase synchronverter for a grid-connected roof top photovoltaic system,"*IET Renew. Power Gener*., vol. 10, no. 8, pp. 1187-1194, 2016, doi: 10.1049/iet-rpg.2015.0224.

[20] H. Ali, and H. A. Khan, "Analysis on inverter selection for domestic rooftop solar photovoltaic system deployment,"*Int. Trans. Electr. Energy Syst*., vol. 30, no. 5, pp. e12351, 2020, doi: 10.1002/2050-7038.12351.

[21] Z. R. Xu, P. Yang, D. B. Zhou, P. Li, J. Y. Lei, and Y. R. Chen, "An improved variable step size MPPT algorithm based on INC,"*J. Power Electron*., vol. 15, no. 2, pp. 487-496, 2015, doi: 10.6113/JPE.2015.15.2.487.

[22] D. N. Dang, T. Le Viet, H. Takano, and T.N. Duc, "Estimating parameters of photovoltaic modules based on current–voltage characteristics at operating conditions,"*Energy Rep.*, vol. 9, pp. 18-26,

2023, doi: 10.1016/j.egyr.2022.10.361.

[23] J. Polo, N. Martín-Chivelet, M. C. Alonso-García, H. Zitouni, M. Alonso-Abella, C. Sanz-Saiz, and N. Vela-Barrionuevo, "Modeling IV curves of photovoltaic modules at indoor and outdoor conditions by using the Lambert function,"*Energy Convers. Manag*., vol. 195, pp. 1004-1011, 2019, doi: 10.1016/j.enconman.2019.05.085.

[24] V. L. Nguyen, , "Couplage des systèmes photovoltaïques et des véhicules électriques au réseau: problèmes et solutions,"Ph.D dissertation, Univ. Grenoble, 2014.